Characterization of the ATP-Binding Domain of the Sarco(endo)plasmic Reticulum Ca^{2+}-ATPase: Probing Nucleotide Binding by Multidimensional NMR†

Mona Abu-Abed,‡ Tapas K. Mal,§ Masatsune Kainosho,|| David H. MacLennan,‡ and Mitsuhiko Ikura*,§

Banting and Best Department of Medical Research, University of Toronto, 112 College Street, Toronto, Ontario, Canada M5G 1L6, Department of Medical Biophysics, University of Toronto, 610 University Avenue, Toronto, Ontario, Canada M5G 2M9, and JST & Graduate School of Science, Tokyo Metropolitan University, Hachioji, Tokyo 192-0397, Japan

Received August 21, 2001; Revised Manuscript Received October 24, 2001

ABSTRACT: The skeletal muscle sarco(endo)plasmic reticulum Ca^{2+}-ATPase (SERCA1a) mediates muscle relaxation by pumping Ca^{2+} from the cytosol to the ER/SR lumen. In efforts aimed at understanding the structural basis for the conformational changes accompanying the reaction cycle catalyzed by SERCA1a, we have studied the ATP-binding domain of SERCA1a in both nucleotide-bound and -free forms by NMR. Limited proteolysis analyses guided us to express a 28 kDa stably folded fragment containing the nucleotide-binding domain of SERCA1a spanning residues Thr357−Leu600. ATP binding activity was demonstrated for this fragment by a FITC competition assay. A nearly complete backbone resonance assignment of this 28 kDa ATP-binding fragment, in both the AMP-PNP-bound and -free forms, was obtained by means of heteronuclear multidimensional NMR techniques. NMR titration experiments with AMP-PNP revealed a confined nucleotide-binding site which coincides with a cytoplasmic pocket region identified in the crystal structure of apo-SERCA1a. These results are consistent with previous site-directed mutagenesis studies of SERCA1a.

Transient increases in intracellular Ca^{2+} levels govern a spectrum of cellular processes in eukaryotic cells, including muscle contraction, fertilization, vesicle trafficking, gene expression, and quality control of protein folding (*1*, *2*). The activation of Ca^{2+} channels in the plasma membrane permits entry of Ca^{2+} from extracellular spaces, while the activation of Ca^{2+} release channels in the sarco(endo)plasmic reticulum permits entry of Ca^{2+} from internal stores. After acting on its intracellular targets, Ca^{2+} is pumped out of the cytoplasm by Ca^{2+}-ATPases (Ca^{2+} pumps) located at the sarco(endo)-plasmic reticulum (SERCA)[1] or plasma membrane (PMCA). Ca^{2+} pumps have the highest affinities for Ca^{2+}, thereby defining resting Ca^{2+} concentrations.

In fast-twitch skeletal muscle, Ca^{2+} released from the sarcoplasmic reticulum through a Ca^{2+} release channel known as ryanodine receptor isoform 1 (RyR1) initiates a contraction cycle. The removal of Ca^{2+}, primarily by the Ca^{2+}-ATPase isoform SERCA1a, rapidly reduces cytoplasmic Ca^{2+} concentrations to resting levels of <100 nM, initiating relaxation and replenishing sarcoplasmic reticulum Ca^{2+} stores in preparation for subsequent cycles of contraction (*3*). Disruption of both copies of the *ATP2A1* gene encoding SERCA1 leads to Brody disease (*4*), an autosomal recessive myopathy characterized by exercise-induced contracture due to a slow rate of removal of Ca^{2+} from the cytosol. The disruption of one copy of the *ATP2A2* gene encoding SERCA2 leads to Darier disease, an autosomal dominant skin disorder characterized by loss of adhesion between epithelial cells, which is associated with breakdown of the desmosomal−filament complex and premature keratinization (*5*). Clearly, these diseases result from aberrant SERCA function (*6*−*8*).

SERCAs translocate Ca^{2+} against a 1000-fold concentration differential (*2*), hydrolyzing 1 mol of ATP per 2 mol of Ca^{2+} that is translocated (*9*). An essential step during the reaction cycle is the phosphorylation of a highly conserved Asp residue, an unusual site for phosphorylation in eukaryotes. Cation ATPases that are phosphorylated by ATP, including the Na^+/K^+-ATPase (*10*) and H^+-ATPase (*11*), are collectively classified as P-type ATPases, since they share numerous mechanistic and structural similarities (*12*, *13*). Kinetic studies have indicated that Ca^{2+}-ATPases undergo conformational changes between two main reactive states (E1 and E2), altering the affinity for Ca^{2+}. In the E1 state,

† This research was supported by Grant MT-12545 to D.H.M. from the Canadian Institutes of Health Research. M.I. is a Howard Hughes Medical Institute International Scholar and a Canadian Institutes of Health Research Scientist. M.A.-A. was supported by a studentship from the Heart and Stroke Foundation of Canada.

* To whom correspondence should be addressed: Department of Medical Biophysics, University of Toronto, 610 University Ave., Toronto, Ontario, Canada M5G 2M9. Telephone: (416) 946-2025. Fax: (416) 946-2055. E-mail: mikura@uhnres.utoronto.ca.

‡ Banting and Best Department of Medical Research, University of Toronto.

§ Department of Medical Biophysics, University of Toronto.

|| Tokyo Metropolitan University.

[1] Abbreviations: 2D and 3D, two- and three-dimensional, respectively; AEBSF, aminoethylbenzenesulfonic acid; ATP, 2′,3′-dideoxyadenosine 5′-triphosphate; AMP-PNP, 5′-adenylylimidodiphosphate; $C_{12}E_8$, octaethylene glycol dodecyl ether; CSI, chemical shift index; HSQC, heteronuclear single-quantum coherence; NOE, nuclear Overhauser effect; NOESY, nuclear Overhauser effect spectroscopy; PCR, polymerase chain reaction; ppm, parts per million; rmsd, root-mean-square deviation; SERCA, sarco(endo)plasmic reticulum Ca^{2+}-ATPase.

10.1021/bi015703n CCC: $22.00
Published on Web 01/03/2002

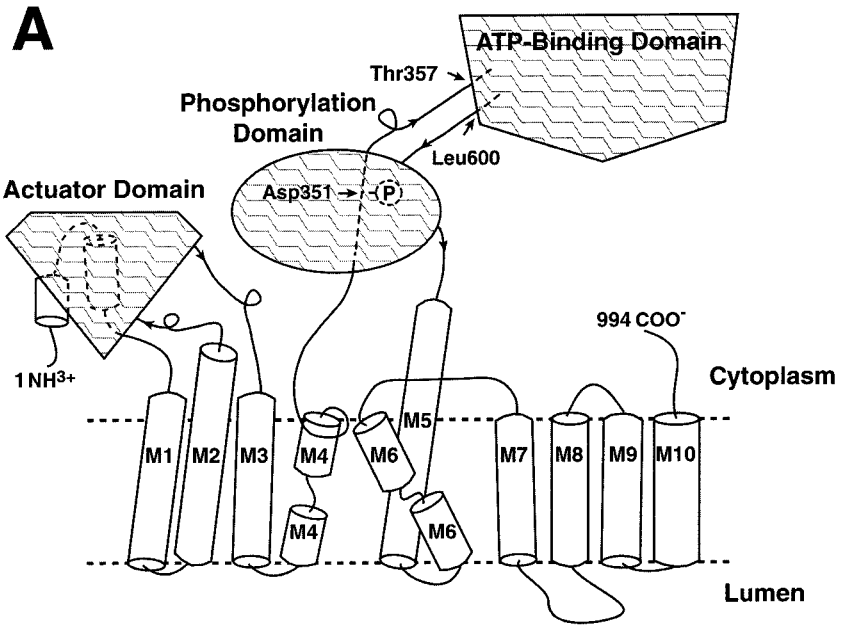

B

```
357          367          377          387          397
 TTNQMSVCKM FIIDKVDGDF CSLNEFSITG STYAPEGEVL KNDKPIRSGQ

407          417          427          437          447
 FDGLVELATI CALCNDSSLD FNETKGVYEK VGEATETALT TLVEKMNVFN

457          467          477          487          497
 TEVRNLSKVE RANACNSVIR QLMKKEFTLE FSRDRKSMSV YCSPAKSSRA

507          517          527          537          547
 AVGNKMFVKG APEGVIDRCN YVRVGTTRVP MTGPVKEKIL SVIKEWGTGR

557          567          577          587          397
 DTLRCLALAT RDTPPKREEM VLDDSSRFME YETDLTFVGV VGML
```

FIGURE 1: (A) Schematic cartoon of the topology of SERCA1a. Transmembrane segments are denoted M1−M10. The location of the ATP-phosphorylatable Asp351 as well as the boundaries of the soluble nucleotide domain [SERCA1a(357−600)] are denoted with arrows. (B) Amino acid sequence of SERCA1a(357−600).

the affinity for Ca^{2+} is 3 orders of magnitude higher than that in the E2 state. While ATP can bind in the presence or absence of Ca^{2+}, phosphorylation of Asp351 by ATP is contingent upon binding of Ca^{2+} to both sites. Phosphorylation by ATP triggers conformational changes leading successively to high- and low-energy states (E1P and E2P, respectively), while dephosphorylation leads to the E2 state. Release of Ca^{2+} into the ER lumen occurs during the transition from E1P to E2P (reviewed in refs *14* and *15*). Structural predictions, based on primary sequence (*16*) and the findings of numerous mutagenesis studies (*17*, *18*), indicated a large separation between the membrane-embedded Ca^{2+} binding sites and the ATP binding and phosphorylation sites which were mapped to cytoplasmic regions. Accordingly, there was speculation that long-range movements must occur through stepwise conformational changes to account for the communication between the Ca^{2+} binding sites and those involved in ATP binding and phosphorylation.

Extensive biochemical analyses of rabbit SERCA1a predicted that this 994-residue protein was comprised of 10 transmembrane segments and 3 cytoplasmic domains: actuator (transduction), nucleotide-binding, and phosphorylation domains (*19*) (see Figure 1). Structural studies of the Ca^{2+} pump using three-dimensional reconstruction from negatively stained 2D crystals or diffraction from frozen tubular structures provided low-resolution "snapshots" of some of the reaction cycle intermediates (*20*−*23*). An 8 Å model of the Ca^{2+}-ATPase in the E2 state illuminated the relative arrangement of the 3 cytoplasmic domains and the 10 transmembrane segments under Ca^{2+}-free conditions (*24*). In a recent landmark study, the structure of SERCA1a in the Ca^{2+}-bound E1 state was reported at 2.6 Å resolution, allowing the resolution of bond-level detail of the cytoplasmic and transmembrane domains (*25*). Understanding of the intricate residue and helix interactions at the Ca^{2+} binding sites was extended considerably by such high-resolution analysis. In addition, the crystal structure showed the association of two helices at the N-terminus of the molecule with a cytosolic β-strand domain between helices M2 and M3 to form an actuator domain and a cytosolic loop between transmembrane helices M6 and M7, which winds around and links several elements of the stalk sector. These two features set up linkages that might involve virtually all of the transmembrane helices in the conformational movements that drive Ca^{2+} transport (*26*).

While the overall shape of the molecule was consistent between the crystal structure and earlier structures, the cytoplasmic domains were widely separated in the 2.6 Å model of the E1 state, in stark contrast to their compact packing in the 8 Å E2 model. Only minor changes were noted in the transmembrane segments. The effects of nucleotide binding were not evident in the crystal structure, however, since the addition of ATP dissolved the crystals. Crystals in which TNP-AMP was infused provided a 4 Å electron

density map that could not conclusively identify changes in the nucleotide-binding domain or the Ca^{2+} binding segments due to low resolution. Therefore, it remains a challenge to gain insight into the conformational changes that occur following ATP binding. Such changes might occur within the nucleotide-binding domain, between nucleotide-binding and phosphorylation domains, and/or within the Ca^{2+} binding sites.

Here we report findings from our solution nuclear magnetic resonance (NMR) studies of a 28 kDa recombinant peptide which constitutes the complete nucleotide-binding domain of SERCA1a, SERCA(357−600). Analysis of the isolated nucleotide-binding domain provides an opportunity to look closely at intradomain conformational changes solely due to interactions with the nucleotide. In this paper, we describe backbone ^1H, ^{13}C, and ^{15}N resonance assignment of residues in this domain and examine nucleotide binding to a nonhydrolyzable ATP analogue.

MATERIALS AND METHODS

Subcloning, Expression, and Purification of the Nucleotide-Binding Domain. Rabbit SERCA1a cDNA encoding the sequence of residues Thr357−Leu600 was amplified by PCR using primers that introduced restriction sites *Nde*I and *Xho*I at the 3′ and 5′ ends, respectively. The PCR protocol that was implemented was in accordance with that of Stratagene's Quick Mutagenesis Kit. The amplified product was concatenated using a Klenow−kinase−ligase reaction (*27*), gel purified, digested, and subcloned between the *Nde*I and *Xho*I restriction sites of the expression plasmid pET15b (Novagen), downstream of the sequence encoding a hexahistidine tag and a thrombin recognition site. This was used to transform *Escherichia coli* strain BL21(DE3) for expression. Bacterial growth was routinely carried out in 1 L of LB medium (unlabeled protein) at 37 °C until an OD_{600} of 0.4 was reached. IPTG was then added to the growing culture to achieve a final concentration of 0.5 mM, and the culture was left for at least 5 h at 37 °C. Cells were harvested by centrifugation for 20 min at 6000 rpm (Sorvall GSA rotor) at 4 °C, and resuspended in 20 mL of ice-cold buffer [25 mM Tris-HCl (pH 8), 500 mM NaCl, 10% glycerol, 5 mM imidazole, and protease inhibitors]. The cell suspension was incubated with 10 mg of lysozyme and 100 μg of DNase I in the presence of 10 mM $MgCl_2$ for 45 min with gentle agitation at 4 °C, and then lysed by sonication on ice. The clear lysate was separated by centrifugation at 100000*g* (Beckman Ti 50.2 rotor) for 30 min. The soluble lysate was applied to 5 mL of Ni−NTA resin (Qiagen), and protein was eluted with buffer containing 500 mM imidazole after extensive column washing. The N-terminal histidine tag was removed by digestion with thrombin.

NMR samples were prepared from modified growth media. Minimal M9 medium supplemented with 1 g/L [^{15}N]NH_4Cl and/or 2 g/L [$^{13}C_6$]glucose was used instead of LB. On occasion, labeling of the protein with ^2H was sought and achieved using 50−99% [^2H]H_2O-based M9 medium, supplemented with the other stable isotopes, as required. [^2H]H_2O-based growth was typically carried out in a 2 L culture that was left overnight at 15 °C after addition of IPTC to ensure good expression levels. Following protein purification, as described above, the sample was exchanged into NMR buffer [20 mM Tris-HCl (pH 7.5), 300 mM NaCl, 200 mM Na_2SO_4, 10 mM DTT, and 1 mM AEBSF] and concentrated by ultrafiltration on a Centricon-10 unit (Amicon). The final protein concentration of NMR samples was 30 mg/mL in a volume of 0.5 mL (∼1 mM).

FITC Labeling Assay. FITC labeling reactions were carried out as described previously (*28*), using a purified protein sample with an uncleaved N-terminal His_6 tag. Briefly, a 0.5 mg/mL protein sample in 50 mM Tris-HCl (pH 7.5) and 20 mM EDTA was incubated with 5 μM FITC in 20 μL of reaction mix at 22 °C for 10 min with or without 5 mM ATP and 2.5 mM $MgCl_2$. No EDTA was included in the reaction mix when ATP or $MgCl_2$ was added. Reactions were stopped by the addition of 20 μL of stop solution [3 volumes of 3× SDS loading dye, 1 volume of 10% SDS, 1 volume of 8 M urea, 1 volume of 100 mM Tris-HCl (pH 8.8), and 0.5% (v/v) β-mercaptoethanol]. Positive control reactions were carried out with rabbit SERCA1a extracted from fast skeletal muscle according to published protocols (*29*) and purified further, as follows. The F3 protein preparation at 10 mg/mL, suspended in 20 mM MOPS (pH 7), 1 mM $CaCl_2$, 1 mM $MgCl_2$, 20% glycerol, and 250 μM DTT, was diluted to 2 mg/mL and solubilized in 0.5% $C_{12}E_8$, vortexed briefly, and then centrifuged at 20000*g* for 10 min at 4 °C. The supernatant fraction was removed and diluted with detergent-free buffer so that the final protein concentration was 0.5 mg/mL in 0.1% $C_{12}E_8$. The resulting preparation ran as a single 94 kDa band on SDS−PAGE and was used in the FITC labeling reactions, as described above, except that the reaction buffer was 20 mM MOPS (pH 7). Reactions in which the protein was mixed with 1% SDS prior to incubation with FITC were included as a negative control. Aliquots of the reaction mixes were loaded on 12 or 8% denaturing polyacrylamide gels under reducing conditions to resolve protein bands. Gels were viewed under UV light to detect FITC-conjugated bands prior to staining with Coomassie blue.

NMR Spectroscopy Experiments. NMR spectra were recorded at 23 °C using a 500 or 600 MHz Varian INOVA spectrometer. $^1H-^{15}N$ heteronuclear single-quantum coherence (HSQC) spectra were measured on a ^{15}N-labeled sample using 128 complex t_1 increments of 1152 data points and 16 transients. Spectral widths were 36 and 14.9 ppm for the ^{15}N (F_1) and ^1H (F_2) dimensions, respectively. A different protein sample that was uniformly labeled with ^2H (>99%), ^{15}N, and ^{13}C was used to record the following triple-resonance experiments: (1) HNCOCA, (2) HNCOCACB, (3) HNCA, and (4) HNCACB (*30*, *31*). These 3D spectra were recorded using 64 complex t_1 increments of 1024 data points and 8 (HNCOCA and HNCOCACB) or 16 (HNCA and HNCACB) transients. NMR data were routinely processed with NMRDraw and NMRPipe (*32*), while the program XEasy (*33*) was used to analyze the spectra.

Secondary structure analysis was performed using the chemical shift index (CSI) method (*34*). CSI calculations were modified to account simultaneously for the $^{13}C\alpha-^{13}C\beta$ resonances and to take into consideration the two flanking residues in the sequence (*35*). A weighted CSI function was used as follows:

$$\mathrm{CSI}(C\alpha_i,C\beta_i) = {}^1/_4[(\Delta C\alpha_{i-1} - \Delta C\beta_{i-1}) + 2(\Delta C\alpha_i - \Delta C\beta_i) + (\Delta C\alpha_{i+1} - \Delta C\beta_{i+1})]$$

where $\Delta C\alpha_i$ and $\Delta C\beta_i$ correspond to the deviation of the observed chemical shift values of the Cα and Cβ atoms, respectively, of residue *i* from the random coil values for the same residue type.

NMR titration experiments entailed acquiring spectra at various protein:ligand ratios to probe gradual changes in the chemical shifts of the protein (or ligand). All titration experiments reported here involved recording 2D spectra that measured either $^1H-^{15}N$ (^{15}N HSQC) or $^1H-^{13}C$ (CT ^{13}C HSQC) correlation. Titration with unlabeled AMP-PNP (Sigma) was carried out with a 1 mM ^{15}N-labeled protein sample. A $^1H-^{15}N$ HSQC spectrum was recorded initially in the absence of AMP-PNP. Then the sample was taken out of the NMR tube and mixed with 2.5 μL of a 100 mM AMP-PNP solution to achieve a nucleotide:protein molar ratio of 0.5:1, before a new $^1H-^{15}N$ HSQC spectrum was recorded. More nucleotide solution was added incrementally to measure HSQC spectra at nucleotide:protein molar ratios of 1:1, 2:1, 4:1, 6:1, and 8:1. The concentration of the protein was not adjusted after each titration point due to the small volume of nucleotide solution that was added. Spectra corresponding to 0:1 and 8:1 nucleotide:protein molar ratios were compared to calculate normalized weighted average chemical shift differences ($\Delta_{ave}/\Delta_{max}$) for the ^1H and ^{15}N chemical shifts of the protein with and without AMP-PNP (*36*). To discern amino acids for which a most significant $^1H-^{15}N$ chemical shift change occurred, three cutoff values above of the mean $\Delta_{ave}/\Delta_{max}$ (calculated from non-zero $\Delta_{ave}/\Delta_{max}$ values) were chosen. Peak changes were categorized into different significance levels: 3-, 2-, and 1.5-fold above the mean.

Titration of an unlabeled protein sample with uniformly ^{15}N- and ^{13}C-labeled AMP-PNP (*37*) was also carried out to investigate changes in the nucleotide due to protein binding. A $^1H-^{13}C$ HSQC spectrum was recorded initially for a 1 mM solution of the labeled nucleotide in the absence of protein. This was mixed with 0.25 equiv of unlabeled SERCA1a(357−600), and a new $^1H-^{13}C$ HSQC spectrum was recorded. Subsequent titration points involved measuring spectra at 1:0.5, 1:0.75, and 1:1 nucleotide:protein ratios. Addition of the protein solution to the nucleotide caused considerable dilution of both, but no adjustment was made to the volume since the molar ratio was preserved. However, the number of transients was increased for the last two titration points to improve the signal-to-noise ratio. All $^1H-^{13}C$ HSQC spectra were recorded using 64 complex t_1 increments of 1024 data points and 8 transients (16 and 24 for the last two titrations). The ^1H, ^{13}C, and ^{15}N chemical shifts have been deposited in BioMagResBank under accession number BMRB-5161.

RESULTS AND DISCUSSION

Delimiting the ATP-Binding Domain. SERCA1a(357−600) constitutes roughly 25% of the full sequence and is located within the large cytoplasmic domain of the Ca^{2+}-ATPase delimited by M4 and M5 (Figure 1). Our limited proteolysis studies and those published by others (*38*, *39*) indicated that this region of SERCA1a forms an independently folded domain readily released by digestion with a variety of proteases. Design of the amino acid boundaries for the minimal sequence of the nucleotide-binding domain was based on the findings of Champeil et al. (*38*) and involved engineering 12 separate constructs varying in size between 28 and 35 kDa, all within the cytoplasmic sequence of SERCA1a. These constructs were designed so that the N-terminus started at Ile348, Asp351, or Thr357 and the C-terminus ended at Ala652, Arg615, Ser610, or Leu600 (data not shown). Small-scale expression in *E. coli* was performed to assess the relative solubilities of these fragments. Optimal solubility properties were found for constructs starting at Thr357 and ending at Leu600. Expression of SERCA1a(357−600) in *E. coli* routinely yielded 15 mg of soluble purified protein per liter of LB medium. SERCA1a(357−600) gave excellent NMR spectra and was selected for further analyses.

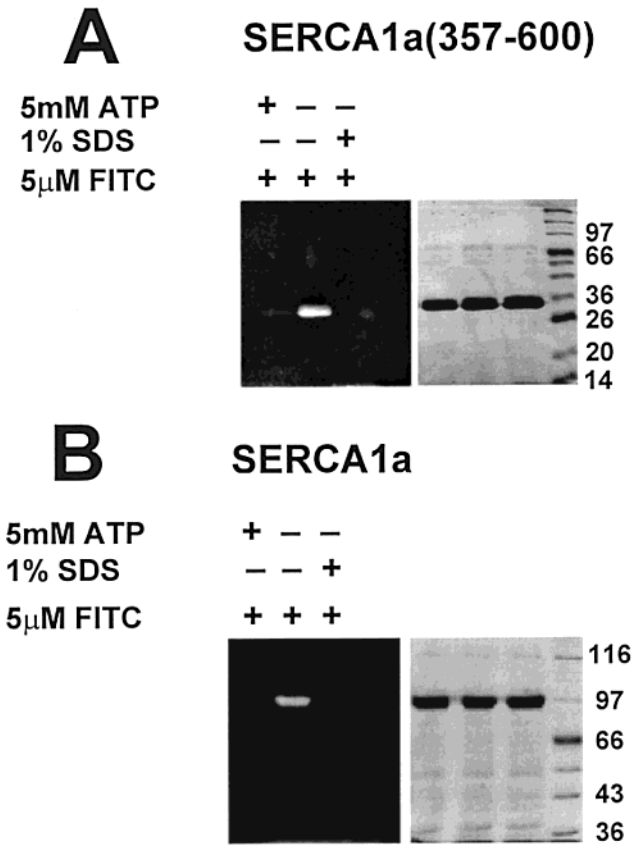

FIGURE 2: FITC labeling assay. Protein samples of (A) SERCA1a(357−600) and (B) SERCA1a at ~0.5 mg/mL were reacted with FITC with or without ATP and with or without 1% SDS for 10 min at room temperature prior to analysis via SDS−PAGE. Gels on the left side were exposed to UV light prior to staining. Bands appearing in white indicate a FITC-labeled sample. The gels were stained with Coomassie blue afterward and appear on the right side.

ATP Binding Assay. The nucleotide binding properties of SERCA1a(357−600) were demonstrated by means of a fluorescein isothiocyanate (FITC) assay. FITC, a known inhibitor of P-type ATPases (*40*), reacts with Lys515 of SERCA1a in the absence of ATP, but is unreactive when ATP is bound. Like the full-length protein, the soluble fragment could be protected from FITC labeling in the presence of saturating amounts of ATP (Figure 2). Lys515 has been identified as the target of the labeling reaction (*40*) and is believed to be within the nucleotide binding pocket, becoming inaccessible to FITC when ATP is bound. It has

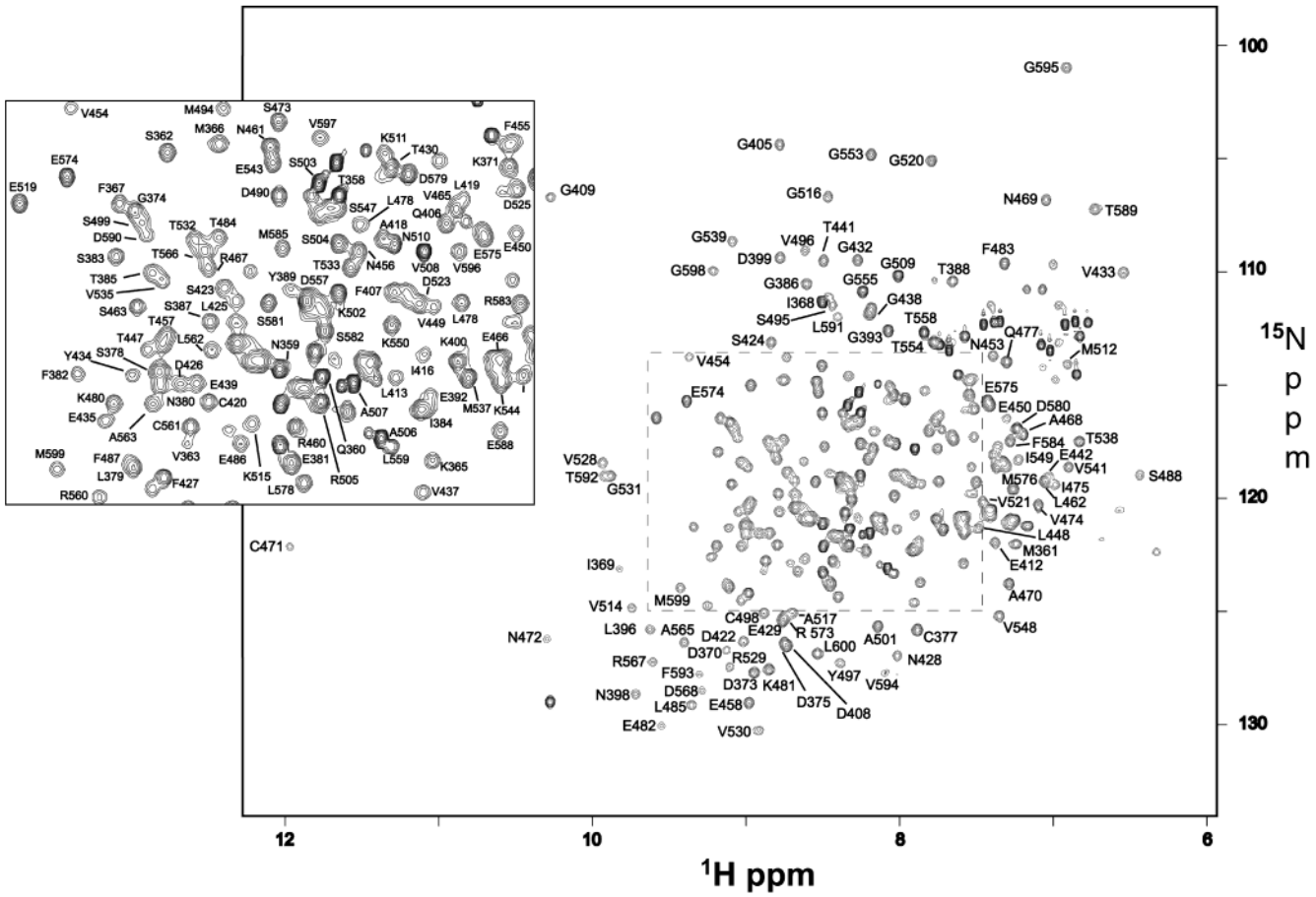

FIGURE 3: ^{1}H−^{15}N HSQC spectrum of SERCA1a(357−600). Backbone peaks are labeled with the amino acid assignments.

not been determined, however, whether Lys515 is involved in direct interactions with the nucleotide. The preservation of ATP binding, albeit with a lower affinity, to this 244-amino acid fragment is clearly illustrated. Detection of residual FITC labeling of SERCA1a(357−600) in the presence of 5 mM ATP (Figure 2A) indicated weaker nucleotide binding compared to that of full-length SERCA1a, and is consistent with previous reports (*38*). In a negative control reaction in which no ATP was present, but 1% SDS was included, no labeling was detected, demonstrating that reactivity toward FITC was contingent upon preservation of the structural integrity of the nucleotide binding pocket. An additional negative control reaction was performed using CTP instead of ATP. Labeling by FITC was unaffected in the presence of CTP (data not shown).

While SERCA1a(357−600) constitutes the nucleotide-binding domain of SERCA1a, it has no ATPase activity on its own since it is mainly involved in interactions with the adenine moiety of ATP (see Nucleotide Binding Studies). Most catalytic residues required for the hydrolysis of ATP are located in the phosphorylation domain (residues 330−356 and 605−737; see Figure 1).

Backbone Assignment and Chemical Shift Analysis. ^{1}H−^{15}N HSQC spectra, representing a fingerprint of the protein backbone, were used in this study as a quick, informative probe of the changes in backbone conformation. Our SERCA1a(357−600) construct contained 244 amino acid residues preceded by a Ser-His-Met N-terminal sequence (from the vector) and included 8 prolines, 12 asparagines, and 3 glutamines. Hence, the expected total number of ^{1}H−^{15}N HSQC peaks was 238 backbone ^{1}H−^{15}N cross-peaks and 15 pairs of cross-peaks from side chain NH_2 groups plus additional side chain cross-peaks from the 18 lysines, 15 arginines, and 1 tryptophan. For the backbone amide groups, 231 resolvable cross-peaks were observed in the HSQC spectrum. These were assigned (Figure 3) after analysis of the 3D triple-resonance spectra. Deuteration was absolutely essential for obtaining high-quality triple-resonance spectra for this 28 kDa protein domain. Backbone assignment has been completed for 94% of the sequence; those remaining unassigned, partly due to peak overlap, are the tripeptide at the N-terminus in addition to Thr357, Ile402, Arg403, Ser404, Ala440, Thr443, Ala444, Leu445, Thr446, Lys492, Ser493, Ile545, and Leu546.

In the CSI method of secondary structure analysis, residues in α-helical regions were distinguished by a local clustering of four or more positive ^{13}Cα−^{13}Cβ CSI values, while those in β-sheet regions were discerned by a local clustering of four or more negative ^{13}Cα−^{13}Cβ CSI values (Figure 4). On the basis of this analysis, we found that SERCA1a(357−600) consists of 12 β-strands and 7 α-helices, consistent with the secondary structure content of the same region of the published 2.6 Å crystal structure (*25*). However, two strands, β6 and β12, seem somewhat shortened or distorted in solution compared to the crystal structure. Strand β12 is at the C-terminus (residues 591−600 in the crystal structure, and 588−592 in solution) and seems partially melted in solution, with the last 8 residues disordered. Strand β6, however, is situated in the middle of the sequence (residues 479−488 in the crystal structure, and 478−480 in solution)

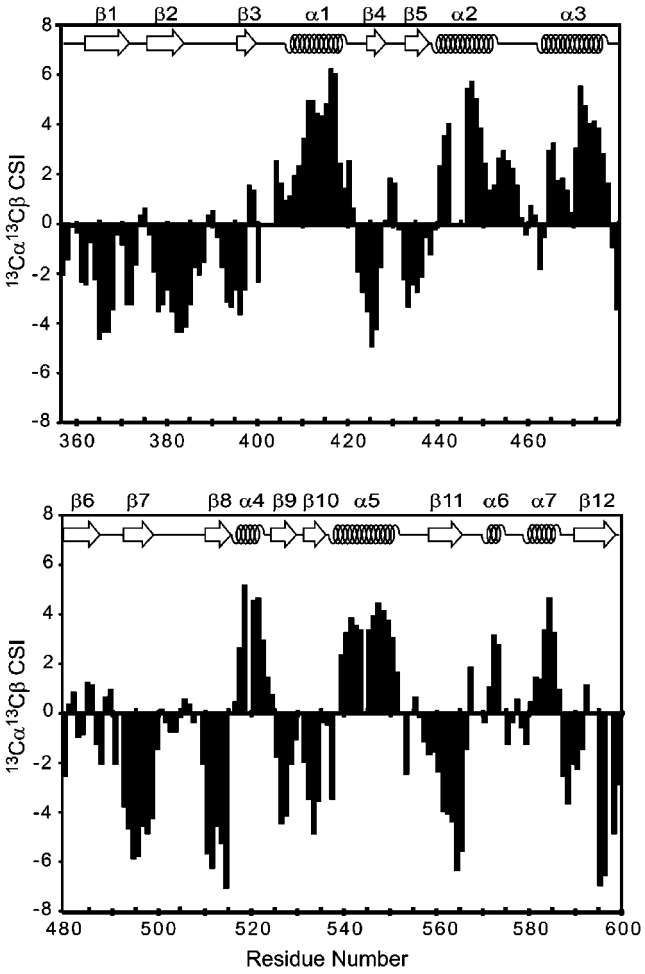

FIGURE 4: $^{13}C\alpha-^{13}C\beta$ chemical shift index plot for assigned residues of SERCA1a(357−600). The first half of the sequence is shown in the top graph, and the remaining residues are included in the bottom graph. Four or more consecutive negative CSI values indicate a β-strand, while four or more consecutive positive CSI values indicate a helix. Zero-CSI regions are random coil sequences. The secondary structure composition of the 2.6 Å crystal structure of SERCA1a (*25*) is plotted next to the *X*-axes; spirals represent helices, while arrows represent β-strands.

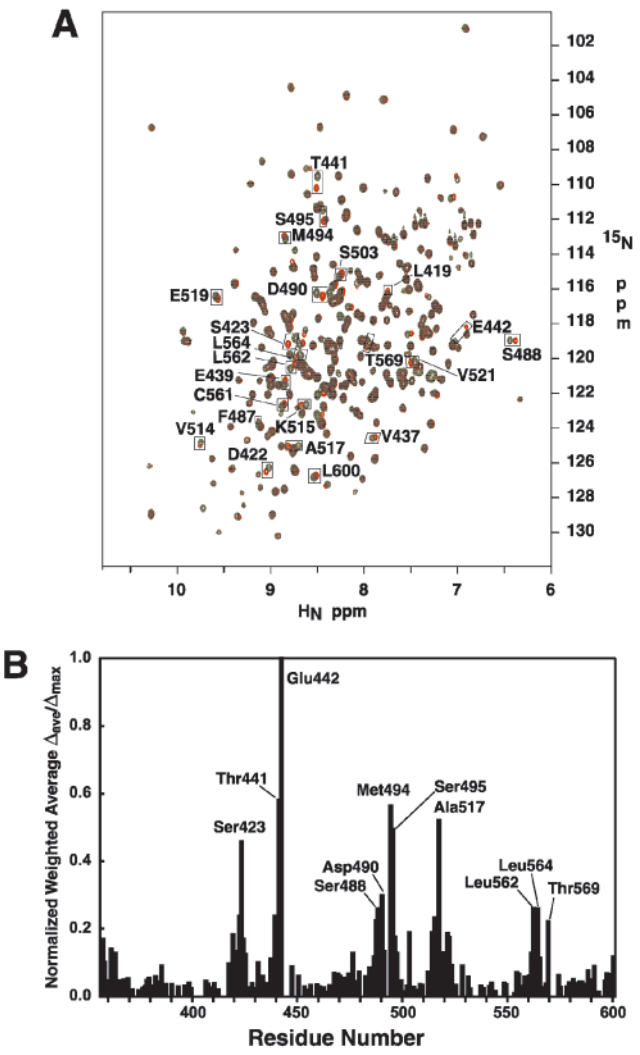

FIGURE 5: (A) Superposition of the ^{15}N HSQC spectra of SERCA1a(357−600) without AMP-PNP (black) or with an 8-fold molar excess of AMP-PNP (red). (B) Normalized weighted average chemical shift differences ($\Delta_{ave}/\Delta_{max}$) for SERCA1a(357−600) upon AMP-PNP binding.

and harbors two nucleotide binding residues, Phe487 and Ser488 (see Nucleotide Binding Studies). Since both cases (crystal structure and our CSI study) studied the protein in the apo form with respect to nucleotide, the distortion of strand β6 around the nucleotide binding residues is thought to be significant, possibly serving to orient these residues specifically in solution. Nonetheless, the boundaries of other strands and helices are essentially identical in the crystal and solution studies, taken within the accuracy limits of CSI analyses. Thus, the overall secondary structure of the nucleotide-binding domain is unchanged in solution relative to that of the crystal structure.

Nucleotide Binding Studies. To map the nucleotide binding site in SERCA1a(357−600), we recorded $^1H-^{15}N$ HSQC spectra with successive addition of AMP-PNP, a nonhydrolyzable analogue of ATP. Addition of the nucleotide produced modest yet significant displacements to a number of HSQC peaks of the protein. The changes in peak positions were observed upon the first addition of the nucleotide (nucleotide:protein molar ratio of 0.5), but were saturated at a nucleotide:protein molar ratio of 6, as no more variations were observed from then onward. Figure 5A shows a superposition of HSQC spectra recorded in the absence of AMP-PNP and in the presence of an 8-fold molar excess of nucleotide. Throughout the titration, the peaks changed in position gradually, representing a fast exchange on the NMR time scale. The relatively high nucleotide:protein ratio required to achieve saturation is indicative of low-affinity nucleotide binding with an estimated K_d in the range from 10^{-5} to 10^{-4} M. In fact, this is consistent with previous results reporting a 20-fold reduction in binding affinity of an isolated nucleotide-binding domain relative to the intact SR Ca^{2+}-ATPase (*38*). Other parts of the Ca^{2+} pump must, therefore, contribute to nucleotide binding. Indeed, residues neighboring Asp351, including but not limited to Lys352, Thr355, and Leu356, are known to be involved in interactions with the phosphate moiety of the nucleotide (*41*, *42*). However, when $^1H-^{15}N$ HSQC spectra were measured in the presence of AMP instead of AMP-PNP, an essentially identical pattern of peak movement was detected (data not shown). The finding that protein binding to AMP is spectrally equivalent to that of AMP-PNP is consistent with early indications that catalytic residues which interact with the distal P_i groups of ATP are located in the phosphorylation domain (*42*) and are

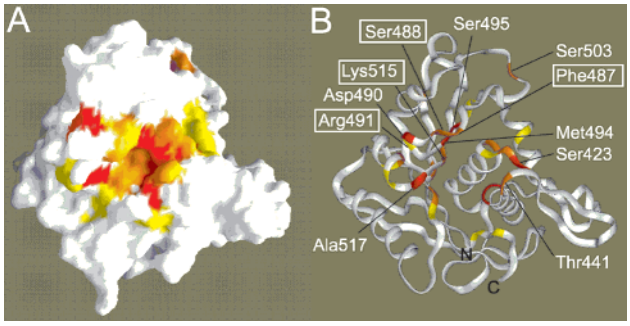

FIGURE 6: Structure of the nucleotide-binding domain of SERCA1a as reported in the 2.6 Å crystal structure (*25*). (A) Surface representation of residues Thr357−Leu600. Highlighted regions correspond to residues for which a change in the $^{1}H-^{15}N$ chemical shift was observed upon binding to AMP-PNP. Residues with the most significant changes (at least 3-fold above average) are colored in red, while those with slightly less significant changes (at least 2- or 1.5-fold above average) are colored in orange and yellow, respectively. (B) Ribbon diagram of the same sequence shown in panel A, showing the identity of some of the residues in the highlighted regions. Mutation sensitive residues are boxed.

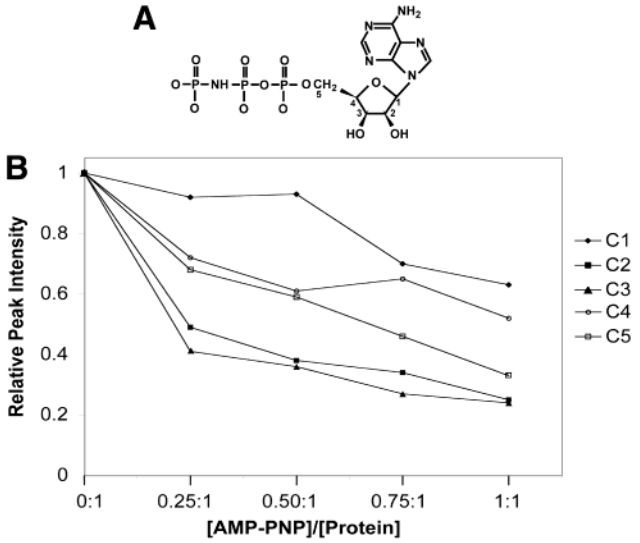

FIGURE 7: (A) Structure of AMP-PNP. (B) Change in the relative peak intensities of carbon atoms of ^{15}N- and ^{13}C-labeled AMP-PNP during titration with SERCA1a(357−600). Peak intensities were normalized for each spectrum relative to a reference non-nucleotide peak.

well-separated from the nucleotide-binding domain (*25*). Accordingly, the observed binding interactions between AMP-PNP and SERCA1a(357−600) represent the essence of the protein−ATP interactions, constituting the core requirements for specific recognition of the adenine moiety.

To quantitate the extent of peak changes, normalized weighted average chemical shift differences ($\Delta_{ave}/\Delta_{max}$) for ^{1}H and ^{15}N chemical shifts of the protein with and without AMP-PNP (see Materials and Methods) were analyzed (Figure 5B). There were 29 amino acids for which a significant $^{1}H-^{15}N$ chemical shift change has been observed. The most significant changes were found for Glu442, Thr441, Met494, Ala517, Ser495, Ser423, and Asp490, which reside in two α-helices (α2 and α4) and two *β*-strands (*β*4 and *β*7). In hopes of gaining insight into the location of these "perturbed" amino acids in the structure, we mapped them onto a surface representation of SERCA1a, utilizing partial coordinates of the 2.6 Å crystal structure that corresponded to the sequence of residues Thr357−Leu600 (Figure 6). The residues with the most significant changes, or highest $\Delta_{ave}/\Delta_{max}$ values (see Figure 5B), are highlighted in accordance with the significance of their chemical shift changes. Amino acids displaying alterations in backbone chemical shifts in the presence of AMP-PNP seemed to cluster about a cavity region in the structure, which is suggestive of the location of the nucleotide-binding pocket.

In the recently determined 2.6 Å structure of SERCA1a in the E1 state (*25*), the authors reported weak diffraction from the TMP-AMP-soaked SERCA1a crystal. The resulting 4 Å map indicated the general location of the nucleotide binding. Residues Lys515, Phe487, Thr441, and Lys492 were determined to be in the proximity of the nucleotide, indicating their potential for interaction with it. The findings of the NMR titration study reported here agree with the preliminary boundaries of the nucleotide binding region outlined in the crystal structure. Moreover, these NMR results extend the boundaries of the binding pocket by identifying further residues influenced by nucleotide binding. Furthermore, on the basis of our preliminary chemical shift and NOE analyses, the secondary structural elements remain unchanged upon AMP-PNP binding. The observed changes in ^{1}H and ^{15}N chemical shifts are probably due to (a) modulation of the environment of HN groups caused by proximity to the nucleotide ligand, (b) local side chain rearrangement, and/or (c) rigid-body movement of a small number of α-helices or *β*-strands with respect to the rest of the molecule.

Investigation of structural similarities between SERCA1a-(357−600) and coordinates deposited in the Protein Data Bank using a combinatorial expansion algorithm resulted in 10 unique structural neighbors. The structural alignment was tenuous, however. The closest structural neighbor that was found was 4-hydroxyphenylpyruvate dioxygenase, upon which 55 residues from SERCA1a(357−600) could be superimposed with an rmsd of 3.4 Å. Interestingly, none of the structural neighbors were nucleotide binding proteins.

Titration of an unlabeled protein sample with ^{15}N- and ^{13}C-labeled AMP-PNP (Figure 7A) was carried out to investigate sites on the nucleotide directly affected by protein binding. Recording a constant time ^{13}C HSQC spectrum of the labeled AMP-PNP allows detection of $^{1}H-^{13}C$ resonances from the ribose ring and C5 only. No changes to the relative peak positions of any of the $^{1}H-^{13}C$ atoms in the ribose ring were observed upon successive additions of the protein (data not shown). Rather, considerable peak broadening was seen for C1−C5 chemical shifts, especially those corresponding to C3 and C5. Peak broadening is manifested by a gradual decrease in relative peak intensities throughout the titration procedure (Figure 7B). This peak broadening is most likely attributed to (i) the reduction of T2 relaxation time due to complex formation with the 28 kDa protein domain and/or (ii) a rapid exchange of the nucleotide due to the low affinity of binding to this protein domain. This is in agreement with the aforementioned observation made by the reverse titration of ^{15}N-labeled SERACA1a(357−600) with unlabeled AMP-PNP.

Comparison with Mutagenesis Data. The large body of site-directed mutagenesis data available on SERCA1a (*7*, *43*−*50*) has identified residues that are important to ATPase activity and allowed dissection of their roles in Ca^{2+} binding, nucleotide binding, phosphorylation, and/or conformational

changes (*41*). The NMR data presented here are in excellent agreement with those previously reported mutations affecting ATP binding. Specifically, Phe487, Ser488, Arg491, and Lys515 are mutation-sensitive residues whose backbone chemical shifts change in the presence of AMP-PNP. Mutagenesis studies have predicted that these residues are directly involved in nucleotide binding due to the effect of their replacement on the apparent K_d of ATP. It is noteworthy that Lys515 has long been identified as the residue protected by ATP from derivatization with FITC, a known inhibitor of the Ca^{2+} pump (*40*), but whose exact role in nucleotide binding remained unclear (*44*). Data from our NMR titration studies suggest that Lys515 contributes to nucleotide binding.

Some mutation sensitive residues (i.e., Cys471, Arg489, Gly516, and Thr547) did not display significant chemical shift changes upon AMP-PNP binding. All of these residues except Thr547 are in the proximity of other residues whose chemical shifts changed upon AMP-PNP binding. This could be reconciled if the specific role of these amino residues involves side chain interactions which could not be measured in our $^1H-^{15}N$ HSQC experiment. Therefore, these interactions would be distant from the backbone region and would not be "felt" in our measurements. Gly516, however, would not be expected to partake in such a side chain interaction, but it is likely that its mutation disrupts the secondary structure configuration of the surrounding region, giving rise to compromised ATPase function. With the preceding residue Lys515, which is mutation sensitive and whose chemical shift changed significantly upon nucleotide binding, Gly516 may indeed be serving a structural role.

Mutation-insensitive residues such as Asp490, Ala517, and Glu519 were seen to experience significant changes to their backbone $^1H-^{15}N$ chemical shifts in the presence of AMP-PNP. There is no conclusive evidence of specific binding interactions between these residues and the nucleotide due to tolerance of mutagenesis at these sites. It is possible that the single mutations at positions 490, 517, and 519 could be compensated for and/or accommodated within the protein and did not have deleterious effects on overall function. Some of the shifts of these residues are indeed significant (e.g., Ala517 and Asp490), implying that relatively large changes in the local magnetic parameters occur in the presence of AMP-PNP.

No mutational studies are available on the remaining residues whose backbone conformation was influenced by nucleotide binding, such as Met361, Val363, Leu419, Asn421, Asp422, Ser423, Ser424, Glu439, Thr441, Glu442, Arg476, Met494, Ser495, Val496, Tyr497, Ser503, Val514, Val521, Ile522, Cys561, Leu562, Leu564, and Thr569. It remains to be seen if introducing mutations at any of these sites would have detrimental effects on SERCA activity. It is likely that only a small subset of these residues would be crucial for maintenance of native ATP binding properties, with the remaining residues having only secondary roles, if any role at all.

CONCLUSIONS

We have overexpressed and purified the ATP-binding domain of the ER/SR Ca^{2+}-ATPase, which corresponds to a 28 kDa protein fragment comprising residues Thr357−Leu600. A large-scale production of SERCA1a(357−600) enabled us to study this functionally essential domain by NMR spectroscopy. Nearly complete backbone ^1H, ^{13}C, and ^{15}N resonance assignments have been obtained for this relatively large protein fragment, providing an excellent probe for the interaction with nucleotide ligands as well as partner proteins [e.g., phospholamban (*51*)]. Such work may include lead compound screening by utilizing the SAR-by-NMR method (*52*) in efforts to develop new therapeutic agents for heart failure that would disrupt the inhibitory interaction between this 28k Da fragment and the cytoplasmic domain of phospholamban (*53*).

Findings from NMR titration of SERCA1a(357−600) with the nonhydrolyzable nucleotide AMP-PNP offer insight into the identity of residues lining the nucleotide binding region, specifying at least 29 amino acids within a confined area. These results are in excellent concordance with site-directed mutagenesis studies and are consonant with the model of the nucleotide-bound state derived from the crystal structure (*25*), presenting more comprehensive evidence for the involvement of other amino acid residues within that region.

Finally, these results strongly suggest that ligand binding does not induce dramatic conformational changes within the ATP-binding domain of SERCA. The secondary structure elements remain essentially identical, and probably no significant tertiary structure rearrangement occurs in the transition from the apo to the nucleotide-bound states. These results support the notion that, while maintaining the same overall structural architecture, the ATP-binding domain undergoes a gross movement with respect to the phosphorylation domain in the transition from the $E1(Ca^{2+})_2$ reactive state to the high-energy $E1(Ca^{2+})_2$−P-ADP state.

ACKNOWLEDGMENT

We thank Dr. Tao Yuan for his help in recording triple-resonance data, Ms. Kyoko Yap for assistance with calculation of the chemical shift indeces, and Ms. Jane Gooding for assistance with manuscript editing.

REFERENCES

1. Berridge, M. J., Bootman, M. D., and Lipp, P. (1998) *Nature 395*, 645−648.
2. Carafoli, E. (1987) *Annu. Rev. Biochem. 56*, 395−433.
3. Lamb, G. D. (2000) *Clin. Exp. Pharmacol. Physiol. 27*, 216−224.
4. Brody, I. A. (1969) *N. Engl. J. Med. 281*, 187−192.
5. Fishman, H. C. (1975) *Arch. Dermatol. 111*, 221−222.
6. Karpati, G., Charuk, J., Carpenter, S., Jablecki, C., and Holland, P. (1986) *Ann. Neurol. 20*, 38−49.
7. MacLennan, D. H., Rice, W. J., and Odermatt, A. (1997) *Ann. N.Y. Acad. Sci. 834*, 175−185.
8. Hu, Z., Bonifas, J., Beech, J., Bench, G., Shigihara, T., Ogawa, H., Ikeda, S., Mauro, T., and Epstein, E. J. (2000) *Nat. Genet. 24*, 61−65.
9. Meissner, G. (1973) *Biochim. Biophys. Acta 298*, 906−926.
10. Rice, W. J., Young, H. S., Martin, D. W., Sachs, J. R., and Stokes, D. L. (2001) *Biophys. J. 80*, 2187−2197.
11. Auer, M., Scarborough, G. A., and Kuhlbrandt, W. (1998) *Nature 392*, 840−843.
12. Kuhlbrandt, W., Auer, M., and Scarborough, G. A. (1998) *Curr. Opin. Struct. Biol. 8*, 510−516.
13. Møller, J. V., Juul, B., and le Maire, M. (1996) *Biochim. Biophys. Acta 1286*, 1−51.
14. Andersen, J. P., and Vilsen, B. (1992) *Acta Physiol. Scand. 607*, 151−159.
15. MacLennan, D. H., Rice, W. J., and Green, N. M. (1997) *J. Biol. Chem. 272*, 28815−28818.

16. Brandl, C. J., Green, N. M., Korczak, B., and MacLennan, D. H. (1986) *Cell 44*, 597−607.
17. Clarke, D. M., Loo, T. W., Inesi, G., and MacLennan, D. H. (1989) *Nature 339*, 476−478.
18. Clarke, D. M., Loo, T. W., and MacLennan, D. H. (1990) *J. Biol. Chem. 265*, 22223−22227.
19. MacLennan, D. H., Brandl, C. J., Korczak, B., and Green, N. M. (1985) *Nature 316*, 696−700.
20. Stokes, D. L., and Green, N. M. (1990) *J. Mol. Biol. 213*, 529−538.
21. Stokes, D. L., and Green, N. M. (1990) *Biochem. Soc. Trans. 18*, 841−843.
22. Toyoshima, C., Sasabe, H., and Stokes, D. L. (1993) *Nature 362*, 467−471.
23. Stokes, D. L., and Lacapere, J. J. (1994) *J. Biol. Chem. 269*, 11606−11613.
24. Zhang, P., Toyoshima, C., Yonekura, K., Green, N. M., and Stokes, D. L. (1998) *Nature 392*, 835−839.
25. Toyoshima, C., Nakasako, M., Nomura, H., and Ogawa, H. (2000) *Nature 405*, 647−655.
26. McIntosh, D. B. (2000) *Nat. Struct. Biol. 7*, 532−535.
27. Lorens, J. B. (1991) *PCR Methods Appl. 1*, 140−141.
28. Gatto, C., Wang, A. X., and Kaplan, J. H. (1998) *J. Biol. Chem. 273*, 10578−10585.
29. MacLennan, D. H. (1970) *J. Biol. Chem. 245*, 4508−4518.
30. Yamazaki, T., Lee, W., Revingtom, M., Mattiello, D. L., Dahlquist, F. W., Arrowsmith, C. H., Muhandriam, D. R., and Kay, L. E. (1994) *J. Am. Chem. Soc. 116*, 6464−6465.
31. Yamazaki, T., Lee, W., Arrowsmith, C. H., Muhandriam, D. R., and Kay, L. E. (1994) *J. Am. Chem. Soc. 116*, 11655−11666.
32. Delaglio, F., Grzesiek, S., Vuister, G. W., Zhu, G., Pfeifer, J., and Bax, A. (1995) *J. Biomol. NMR 6*, 277−293.
33. Bartels, C. H., Xia, T.-H., Billeter, M., Güntert, P., and Wüthrick, K. (1995) *J. Biomol. NMR 5*, 1−10.
34. Wishart, D. S., and Sykes, B. D. (1994) *J. Biomol. NMR 4*, 171−180.
35. Spera, S., and Bax, A. (1991) *J. Am. Chem. Soc. 113*, 5490−5492.
36. Foster, M. P., Wuttke, D. S., Clemens, K. R., Jahnke, W., Radhakrishnan, I., Tennant, L., Reymond, M., Chung, J., and Wright, P. E. (1998) *J. Biomol. NMR 12*, 51−71.
37. Tanaka, T., Saha, S. K., Tomomori, C., Ishima, R., Liu, D., Tong, K. I., Park, H., Dutta, R., Qin, L., Swindells, M. B., Yamazaki, T., Ono, A. M., Kainosho, M., Inouye, M., and Ikura, M. (1998) *Nature 396*, 88−92.
38. Champeil, P., Menguy, T., Soulie, S., Juul, B., de Gracia, A. G., Rusconi, F., Falson, P., Denoroy, L., Henao, F., le Maire, M., and Moller, J. V. (1998) *J. Biol. Chem. 273*, 6619−6631.
39. Moutin, M. J., Rapin, C., Miras, R., Vincon, M., Dupont, Y., and McIntosh, D. B. (1998) *J. Biol. Chem. 251*, 682−690.
40. Mitchinson, C., Wilderspin, A. F., Trinnaman, B. J., and Green, N. M. (1982) *FEBS Lett. 146*, 87−92.
41. Andersen, J. P. (1995) *Biosci. Rep. 15*, 243−261.
42. McIntosh, D. B., Woolley, D. G., MacLennan, D. H., Vilsen, B., and Andersen, J. P. (1999) *J. Biol. Chem. 274*, 25227−25236.
43. MacLennan, D. H., Brandl, C. J., Korczak, B., and Green, N. M. (1987) *Soc. Gen. Physiol. Ser. 41*, 287−300.
44. Maruyama, K., and MacLennan, D. H. (1988) *Proc. Natl. Acad. Sci. U.S.A. 85*, 3314−3318.
45. Maruyama, K., Clarke, D. M., Fujii, J., Inesi, G., Loo, T. W., and MacLennan, D. H. (1989) *J. Biol. Chem. 264*, 13038−13042.
46. Maruyama, K., Clarke, D. M., Fujii, J., Loo, T. W., and MacLennan, D. H. (1989) *Cell Motil. Cytoskeleton 14*, 26−34.
47. McIntosh, D. B., Woolley, D. G., Vilsen, B., and Andersen, J. P. (1996) *J. Biol. Chem. 271*, 25778−25789.
48. MacLennan, D. H., Clarke, D. M., Loo, T. W., and Skerjanc, I. S. (1992) *Acta Physiol. Scand. 607*, 141−150.
49. MacLennan, D. H., and Toyofuku, T. (1992) *Biochem. Soc. Trans. 20*, 559−562.
50. MacLennan, D. H., Toyofuku, T., and Lytton, J. (1992) *Ann. N.Y. Acad. Sci. 30*, 1−10.
51. MacLennan, D. H., Toyofuku, T., and Kimura, Y. (1997) *Basic Res. Cardiol. 1*, 11−15.
52. Shuker, S. B., Hajduk, P. J., Meadows, R. P., and Fesik, S. W. (1996) *Science 274*, 1531−1534.
53. Johnson, R. G., Jr. (1998) *Ann. N.Y. Acad. Sci. 853*, 380−392.

BI015703N